

Inferring physical laws by artificial intelligence based causal models

Jorawar Singh,^{1,*} Kishor Bharti,^{2,†} and Arvind^{1,3,‡}

¹*Department of Physical Sciences, Indian Institute of Science Education and Research (IISER) Mohali, Sector 81 SAS Nagar, Manauli PO 140306 Punjab, India*

²*Institute of High Performance Computing (IHPC), Agency for Science, Technology and Research (A*STAR), 1 Fusionopolis Way, #16-16 Conneris, Singapore 138632, Republic of Singapore*

³*Punjabi University, Patiala, 147002, Punjab, India*

The advances in Artificial Intelligence (AI) and Machine Learning (ML) have opened up many avenues for scientific research, and are adding new dimensions to the process of knowledge creation. However, even the most powerful and versatile of ML applications till date are primarily in the domain of analysis of associations and boil down to complex data fitting. Judea Pearl has pointed out that Artificial General Intelligence must involve interventions involving the acts of doing and imagining. Any machine assisted scientific discovery thus must include causal analysis and interventions. In this context, we propose a causal learning model of physical principles, which not only recognizes correlations but also brings out causal relationships. We use the principles of causal inference and interventions to study the cause-and-effect relationships in the context of some well-known physical phenomena. We show that this technique can not only figure out associations among data, but is also able to correctly ascertain the cause-and-effect relations amongst the variables, thereby strengthening (or weakening) our confidence in the proposed model of the underlying physical process.

I. INTRODUCTION

Artificial Intelligence (AI), specifically through its Machine Learning (ML) form, has been successfully applied to a wide range of fields including agriculture, social media, gaming, and robotics [1, 2]. ML plays a significant role in autonomous driving, natural language processing, finance, health care, understanding the human genome, manufacturing, energy harvesting, and much more [2, 3].

ML has also lent a hand to the scientific community and has found quite a few applications in scientific research. In physics specifically, ML has been used to explore many-body physics [4, 5], glassy dynamics [6], learning phases of matter [7–9], designing new experiments [10–13], to interpret nature [14, 15], quantum foundations [16], quantum state tomography [17, 18], phase transition [19, 20], quantum matter [21], Monte Carlo simulation [22], polymer states [23], topological codes [24], the study of black hole detection [25], quantum circuit optimization and control [26, 27], anti-de Sitter/conformal field theory (AdS/CFT) correspondence [28], quantum state preparation [29, 30], thermodynamics [31], gravitational lenses [32], characterizing the landscape of string theories [33], and wave analysis [34], to name a few. An important aim for machine-assisted scientific discovery, proposed in the

seminal work by Iten *et. al.* where they propose a neural network architecture modeled after the human physical reasoning process [35].

The currently prevalent ML architectures primarily identify correlations and associations in data and thus the models only uncover direct connections in the data. Based on the associations one must learn the causal model and the general AI systems should be able to uncover the underlying causal structures. Therefore, to fully realize the potential of artificial general intelligence, one needs to incorporate the essence of cognition within the scope of ML. Judea Pearl [36] divides this cognitive ability into three distinct levels as depicted in Fig. 1, distinguished by the type of query being answered, the levels are termed as: Association, Intervention, and Counterfactuals.

The first level (association) of the ladder described in Fig. 1 involves predictions based on passive observations of the data, *i. e.* data-centric search for correlations, associations, regularities and patterns. This level answers queries pertaining to observations as to what can be found in the data. The second level (intervention), involves analysis of response to change in variables. Rather than just observing the data, one queries the effect of an induced change, and thus one is looking at a cause-and-effect relationship in the variables of the data. The final level utilizes the causal structure to estimate portions of data that don't exist or cannot be observed. It answers queries related to the hypothetical questions that one may imagine - the "what if" questions. Therefore this level involves Counterfactuals.

One thus sees that most applications of ML in sci-

* ph19023@iisermohali.ac.in

† kishor.bharti1@gmail.com

‡ arvind@iisermohali.ac.in

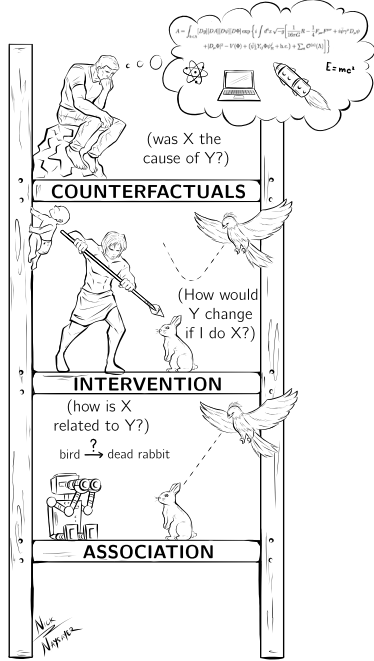


FIG. 1: The Ladder of Causation depicting the 3 levels of cognitive ability. Present day ML is at ‘association’, the lowest level. A machine capable of understanding causal structures would be placed at ‘intervention’ level while the more sophisticated AI will also operate at the level of contrafactuals

ence are basically at the first level of the ladder. For example, in the context of the spring-mass vibrating system, ML can find the relationship between the length of the spring and the weight attached to it. However ML models cannot answer the question, “is the change in spring length caused by the change in weight or vice-versa”. Causal Inference takes us a step above on the ladder of causation and lets us answer such questions. Once armed with the knowledge of causal relations, one can begin exploring the counterfactuals leading to a framework which then becomes a motif for formulating the laws of nature. Posed a bit differently: “Had the weight on this spring doubled, its length would have doubled as well” (Hooke’s law). - Judea Pearl [36].

We begin by studying the basics of causal discovery and causal inference in Section-II. In Section-III we analyze the causality relations of some physical phenomenon. The examples that we consider include tide height, Ohm’s law, light dependent resistance (LDR) characteristics, and quantum measurement correlations. Finally, we close with a discussion on the results and possible paths ahead, in Section-IV.

II. CAUSAL DISCOVERY AND INFERENCE

Causal inference refers to the process of answering questions based on the underlying causal model of the cause-and-effect relationship between different variables of the data. As seen from the ladder of causation (Fig. 1), causality relates to response to interventions. We do a certain action and observe a certain response.

The limitations of correlations and importance of causal relations can be easily understood from a simple experiment of the atmospheric pressure reading of a barometer [36]. While there is a direct correlation between the barometer reading and pressure, this correlation cannot in itself establish the causal relationship. Is it the barometer reading that causes the atmospheric pressure to change or is it the atmospheric pressure that causes the barometer reading to change? One requires the knowledge of causal relations to conclude that it is the pressure that causes the change in reading leading to the observed correlation and not the other way around.

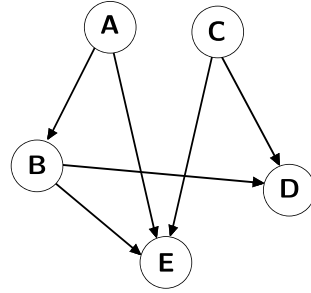


FIG. 2: A directed acyclic graph with nodes representing variables and arrows showing the cause-and-effect relationship between variables.

Statistical algorithms are used to infer the causal structure from observational data. The model is assumed to be **acyclic** where a Directed Acyclic graph(DAG) can be used to depict the causal relationships as shown in Fig. 2. The nodes represent the variables and arrows depict the cause-and-effect relations. The model is considered to be **Markovian** where a given node is conditioned on its immediate parents only. The model is assumed to satisfy the conditions of **Sufficiency** and **Faithfulness** which respectively mean that there exists no external common cause to any pair of nodes in the graph and all conditional independences (from the underlying distribution) are completely represented in the graph. Most algorithms for causal discovery work with the assumption that statistical independence implies the absence of causal rela-

tion [37]. Specifically, the Peter Spirtes and Clark Glymour(PC) algorithm uses the conditional independence testing criterion to generate a DAG from a fully connected graph [38], while the Greedy Equivalence Search(GES) algorithm applies a greedy search in the graph space to fill an empty graph while maximizing a fitness measure [39]. Exploiting the asymmetries in models, LiNGAM (Linear non-Gaussian Acyclic Models) prioritizes the models that better fit a Linear Non-Gaussian relation among the variables [40]. The final goal of causal discovery process is to arrive at the DAG from the given data set.

The standard statistics works with correlations which means working with probability of Y given X denoted by $P(Y|X)$. Causal inference on the other hand works with probability of Y given that X is done denoted by $P(Y|do(X))$ - the do-calculus [36]. This 'do', though a small change from statistics, is the representation of an intervention. The difference from standard ML predictions is that here we are approximating the effect of treatment X on the outcome Y , based on data that does not exist in the data-set.

The basic idea behind causal inference is to estimate the effect of treatment X on the outcome Y while eliminating the dependence on any variable Z that has a direct influence on both the treatment and the outcome (confounding variables). This is schematically explained in Fig. 3. Many methods exist for the estimation of the effect that is produced by doing X . These include observational studies (conducting and simulating randomized experiments), simple natural experiments, instrument variables (specific causal effect estimation criteria) and refutations. These methods are explained in detail in Reference [41].

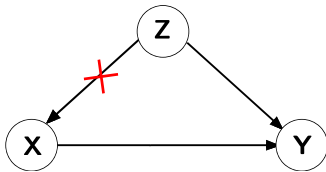


FIG. 3: Basic aim of causal inference is to estimate the effect of a treatment X on the outcome Y while controlling for the confounding variables Z

We use Causal Discovery Toolkit (CDT) [42] to obtain causal models directly from the data and DoWhy, “An end-to-end library for causal inference” [43], to carry out the causal analysis.

The basic analysis involves the following steps:

1. Creating a causal model: We create an initial model of the phenomena that we are studying as a Directed Acyclic Graph. The DAG is input into the DoWhy library as a dot graph (a textual represen-

tation of the graph using DOT Language) [44]. This initial model is either extracted from the data using CDT or from domain knowledge.

2. Causal effect identification: Based on causal model, we identify the causal effects to be estimated using a suitable criterion among the following:

a: Back-door: Controlling for the set of variables that block all the back-door paths between the treatment and the outcome. A Back-door path is any path connecting treatment to outcome via an arrow inward on the treatment. In Fig. 4, $X \leftarrow Z \rightarrow Y$ is a back-door path from treatment X to outcome Y . Adjusting for the variable Z will be the back-door criterion:

$$P(Y|do(X)) = \sum_z P(Y|X, z)P(z)$$

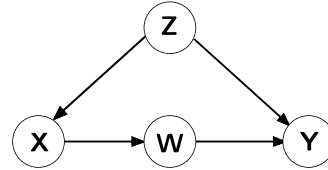


FIG. 4: A sample causal model as a DAG. X is the treatment, Y the outcome, Z a confounder, and W a mediator. $X \leftarrow Z \rightarrow Y$ constitutes the backward path while $X \rightarrow W \rightarrow Y$ is the forward path from treatment to outcome

b: Front-door: Controlling of variables in the forward path from the treatment to outcome. In Fig. 4, $X \rightarrow W \rightarrow Y$ is the front-door path from treatment to outcome. Adjusting for variables X and W will be the front-door criterion:

$$P(Y|do(X)) = \sum_w P(w|X) \sum_x P(Y|x, w)P(x)$$

c: Instrumental variables [41]: A special case of the front-door criteria, this method helps in identifying the direct causal estimate from X to Y when the back-door criterion fails (e.g. - obtaining data on Z is not possible, and hence Z cannot be controlled for). This method can only be applied if there exists a variable which is independent of confounders of treatment and outcome, has a direct relation with the treatment, and has no direct effect on the outcome as depicted in Fig. 5.

d: Mediation: This method is applied when the treatment has multiple causal pathways to the

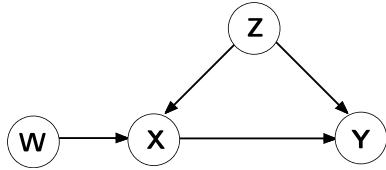


FIG. 5: Causal model for Instrumental Variable. Since W is independent of confounder Z , and has direct effect on treatment X , and has no direct effect on the outcome Y , it can be used to estimate the effect of X on Y (given that controlling for Z is not possible)

outcome as shown in Fig. 6. It enables us to separate the total effect on Y into direct ($X \rightarrow Y$) and indirect ($X \rightarrow W \rightarrow Y$) causal estimates.

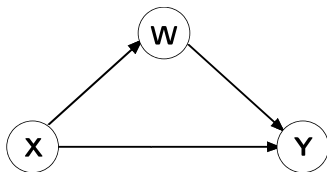


FIG. 6: Mediation causal model. The treatment X has two causal pathways to the outcome Y , direct ($X \rightarrow Y$) and indirect ($X \rightarrow W \rightarrow Y$) via the mediator W

3. Estimate the target estimand: Many statistical methods exist for estimating the identified causal effect. Depending on the identification criteria one can use linear regression, distance matching, propensity score stratification [45] for backdoor; wald estimator [46], regression discontinuity [47] for instrument variable; two-stage linear regression for frontdoor and so on. The estimate is obtained in units of Average Treatment Effect (ATE), Average treatment effect for the treated (ATT) or Average treatment effect for the controls (ATC).

4. Refute the obtained estimate using multiple robustness checks: Causal models are not absolute, as they cannot be proven to be correct or incorrect. One can however, increase faith in a model by checking the validity of the assumptions behind the model against various robustness checks which include:

- a: Random Common Cause:** Check the variation of estimate over addition of an independent random common cause. Lesser the variation, higher our faith in the model.
- b: Placebo Treatment Refuter:** Rerunning the analysis with an independent random variable as the treatment variable. If the initial

treatment is in fact the cause, the new estimate should go to zero.

- c: Data Subset Refuter:** How much is the variation in estimate when only a subset of the data is used? The variation is small for a strong causal relation.

III. EXAMPLES

This section describes our main work where we have chosen four different examples to build causal models. For each case we consider different possible causal models and evaluate their relative efficacy by employing the methods described above. The examples are chosen from diverse fields. The first example of tides and cause of their varying height over the year is about a natural phenomenon where data is taken from documented sources. The second example is about a physics model involving Ohm's law and direct and indirect dependence of current on various possible parameters. The third example is about an actual experiment where we collect data for a light dependent resistance(LDR) and consider various possible causal models for it, which we evaluate and compare using data and domain knowledge. In the last example we consider quantum correlations in the two-party two-value setting, and ask the question as to what is the most plausible cause of these non-trivial quantum correlations.

A. Height of Tides

It is a well known fact that tides, the rise and fall of sea levels, are a cumulative effect of Sun and Moon's gravitational force on Earth, among other minor factors. We ask a ML model, which of the two - **Sun** or **Moon** - plays a bigger role in determining the maximum height of the tide on a given day. To that end, we prepare a data-set with daily Earth-Sun distance in astronomical units(AU), Earth-Moon distance (in AU), and the maximum height of tide at four different locations- Honolulu (Hawaii), Mumbai (India), Liverpool (England), Halifax (Canada)

We collected the year round data of earth-moon distance, earth-sun distance, and tide height from documented sources. The **earth-sun** distance for a given day of the year is obtained from the csv file available on the [USGS webpage](#). A sample of the dataset is shown in Fig. 7

The **earth-moon** distance is extracted from **IM-CCE VIRTUAL OBSERVATORY**. Fig. 8 shows the sample of the table generated at the webpage. The data of **tide height** is available as PDF file on the

DOY	d (AU)	DOY	d (AU)	DOY	d (AU)
47	0.9879406	94	1.0001183	141	1.012103
48	0.9881439	95	1.0004053	142	1.0122969
49	0.9883506	96	1.0006922	143	1.0124871
50	0.9885609	97	1.0009789	144	1.012674
51	0.9887745	98	1.0012652	145	1.0128571
52	0.9889913	99	1.0015508	146	1.0130363
53	0.9892117	100	1.0018362	147	1.0132118
54	0.9894352	101	1.0021209	148	1.0133833

FIG. 7: Sample Earth-Sun distance data. The data includes day of the year (**DOY**) and the Earth-Sun distance d (in AU)

Target	Date	RA "h.m.s"	DEC "d.m.s"	Distance au	M
Moon	2021-08-12T00:00:00.00	12 14 22.22900	+03 26 52.7544	0.002517587	-7.
Moon	2021-08-13T00:00:00.00	13 04 8.31981	-02 32 26.7451	0.002501666	-8.
Moon	2021-08-14T00:00:00.00	13 54 52.12751	-08 28 6.6534	0.002488661	-8.
Moon	2021-08-15T00:00:00.00	14 47 37.25048	-14 01 13.4349	0.002478572	-9.
Moon	2021-08-16T00:00:00.00	15 43 1.29428	-18 51 31.1579	0.002471552	-9.
Moon	2021-08-17T00:00:00.00	16 41 19.45503	-22 37 58.4415	0.002467992	-10
		17 41	-25 01		

FIG. 8: Sample Earth-Moon distance data, 2019. The website generates the ephemeris data for the Moon.

NOAA website. Fig. 9 shows a sample of the PDF. At any given day, the tide heights were recorded 3-4 times. We used the maximum value of height (in ft) for a given day.

January			February		
Time	Height		Time	Height	
1 Tu	0102 19.2 586 0722 7.8 239 1333 19.5 595 1958 7.4 225		16 W	0616 9.3 282 1227 18.3 557 1852 8.6 262	
2 W	0205 19.8 603 0826 7.3 223 1433 20.0 609 2055 6.9 210		17 Th	0103 18.5 564 0728 8.5 259 1337 19.1 581 1958 7.6 233	
3 Th	0259 20.5 625 0921 6.6 202 1524 20.5 625 2145 6.4 194		18 F	0208 19.7 599 0833 7.3 221 1440 20.3 618 2059 6.4 195	
4 F	0346 21.2 647 1008 6.0 184 1608 21.0 640 2228 6.0 182		19 Sa	0306 21.1 642 0931 5.7 174 1537 21.6 659 2153 5.1 154	
5 Sa	0428 21.8 664 1049 5.6 170 1647 21.3 650 2307 5.7 174		20 Su	0400 22.5 686 1024 4.2 129 1628 22.9 697 2244 3.9 118	
			1 F	0239 19.3 587 0903 7.7 236 1509 19.2 585 2128 7.4 227	16 Sa
			2 Sa	0330 20.2 615 0953 6.9 209 1555 20.0 610 2213 6.7 203	17 Su
			3 Su	0413 21.0 641 1035 6.1 185 1634 20.7 631 2252 6.0 184	18 M
			4 M	0450 21.7 661 1111 5.5 167 1708 21.2 646 2327 5.6 170	19 Tu
			5 Tu	0525 22.1 675 1145 5.1 154 1740 21.5 656	20 W

FIG. 9: Sample Tidal data for Liverpool, England, 2019. Each box of a given date records the time (in hours and minutes) height of high and low tides (in feet and cm)

We prepared the models as described in Fig. 10 and computed two causal estimates with tide-height

as the outcome. We used the Earth-Moon distance as target for the first estimate and Earth-Sun distance for the second.

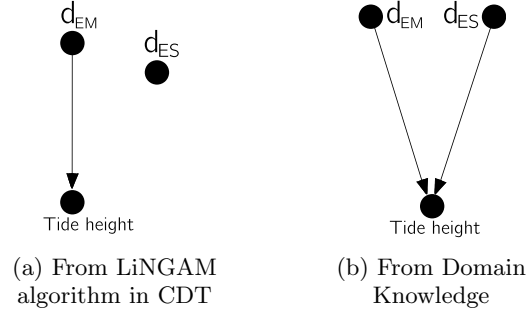


FIG. 10: Causal diagram for tide height. d_{ES} and d_{EM} represent the earth-sun and earth-moon distance respectively

The causal diagram predicted from data only gives us the $d_{EM} \rightarrow h$ causal relation, which is in fact the most significant one. The estimates (in ATE) from the predicted and ground-truth models differ marginally: -2964.45 and -2913.16 respectively (for Halifax). The causal-estimates for Earth-Moon and Earth-Sun distance (in ATE) for the ground-truth model are listed in table I. It is clearly visible from

Causal Relation	Estimate (ATE)			
	Halifax	Liverpool	Honolulu	Mumbai
$d_{EM} \rightarrow h$	-2913.16	-10045.83	-1205.91	-7232.59
$d_{ES} \rightarrow h$	-2.20	-8.62	-3.34	-22.15

TABLE I: Causal estimates for $d_{EM} \rightarrow h$ and $d_{ES} \rightarrow h$ at the four locations. The ATE values are shown for Earth-Moon and Earth-Sun for all four locations.

the estimates and from the causal diagram obtained from data, that the Earth-Moon distance is the primary cause for the tide height.

B. Ohm's law

In this example, we look for the driving forces (cause) of the current I in a wire of length L , cross-sectional area A , resistivity ρ , at a temperature T , with a potential V applied across its ends. Using causal analysis one can test the validity of a given cause and effect relation. To that end, we consider and check the validity of a model with a direct $T \rightarrow I$ arm added in addition to the known dependence of I on T via R . Different causal-models that we evaluate are depicted in Fig. 12.

Using the known relations (Eq. (1)) between current and voltage, and the temperature dependence of resistance, we generate the required data. We use platinum as the material for our constants (α, ρ_0). Fig. 11 shows a sample input data.

$$\begin{aligned} V &= IR \\ R &= \frac{\rho_t L}{A} \\ \rho_t &= \rho_0(1 + \alpha \Delta T) \end{aligned} \quad (1)$$

T	rho	length	r	R	V	I
350.33	2.44E-07	41025.67	0.07	0.66	196.88	297.43
409.38	2.68E-07	78973.99	0.03	10.57	130.91	12.38
472.40	2.94E-07	21563.38	0.03	2.04	183.42	90.04
317.41	2.30E-07	26771.04	0.03	2.90	103.97	35.79
347.62	2.42E-07	13614.24	0.09	0.12	188.06	1564.47
304.76	2.25E-07	93920.52	0.07	1.48	95.37	64.36
410.93	2.69E-07	47551.55	0.03	3.54	122.39	34.54
430.19	2.77E-07	88597.63	0.01	102.67	44.13	0.43
347.70	2.42E-07	62485.56	0.06	1.28	100.53	78.81
361.47	2.48E-07	84994.46	0.02	15.89	217.53	13.69

FIG. 11: Sample of the data-set used in the analysis. Current I resulting from Potential V applied across a wire of length L , resistance R (resistivity ρ , cross-section area A) at temperature T

The candidate causal models depicted in Fig. 12 are evaluated and estimates in terms of ATE values are computed which are tabulated in Table II. We see that the major driving force is potential V , with resistance showing an inverse relation as expected.

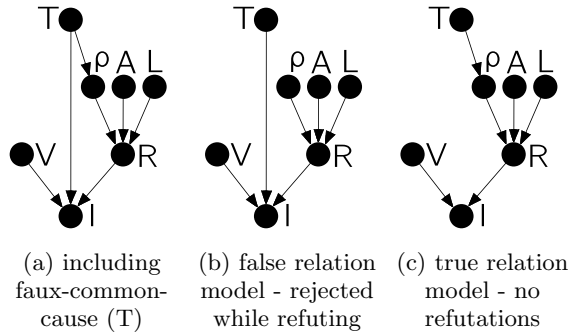


FIG. 12: Causal diagram for Ohm's law. For a wire with potential V across its length L , resistivity ρ , cross-section area A at temperature T

We observe that the effect of T on I is not only non-zero, but equivalent to that of R . The fact that this effect follows not from the direct $T \rightarrow I$ path, but the $T \rightarrow \rho \rightarrow R \rightarrow I$ path is confirmed by estimating the same effect of T on I using a causal model which does not have the $T \rightarrow I$ path (Fig. 12c). We get the same ATE value of 0.218.

One can also check the effect by removing the other branch: $T \rightarrow \rho$ (Fig. 12b). This results in an estimate(ATE) of 1.35, but during the placebo treatment refutation, the new estimated effect in terms of ATE values, which should be 0, comes out to be -10.54 and thus shows that this model is less trustworthy.

Causal Relation	Estimate (ATE)		
	Model A	Model B	Model C
$V \rightarrow I$	1.735	1.735	1.735
$R \rightarrow I$	-0.205	-0.225	-0.205
$T \rightarrow I$	0.218	1.35	0.218

TABLE II: Causal estimates for different causal relations in the three models of Ohm's Law

C. Power and LDR Resistance

Next we perform causal analysis of real data obtained from an experiment. A light emitting diode(LED) light source, runs using a battery at voltage V and draws current I . The light emitted by the LED shines on and light dependent resistance(LDR) and this provides power P to LDR thereby changing its resistance R . The circuit is described in Fig. 13.

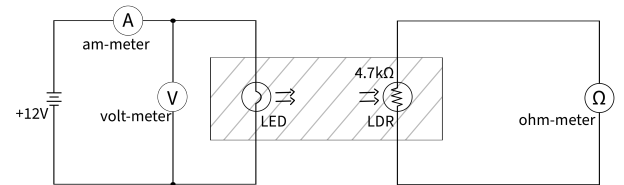


FIG. 13: Circuit Diagram for the LDR Experiment. The LED and LDR are placed in a closed box at a fixed distance from each other. The LED is supplied with a variable voltage. The voltmeter measures the voltage across the LED, the ammeter measures the current through the LED, and the ohmmeter measures the resistance of LDR. The experiment is repeated with flux meter in place of LDR to obtain power readings.

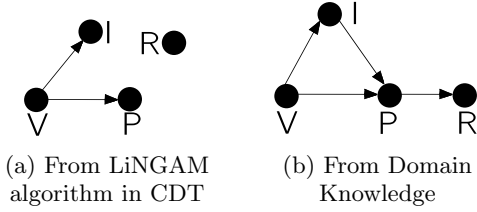


FIG. 14: Causal diagrams for the LDR experiment.

Voltage (V)	Current (mA)	Power (lux)	Resistance (k Ω)
2.67	100.3	5	37.000
2.90	104.7	9	25.400
3.17	109.9	15	17.800
3.68	119.2	36	6.800
3.84	122.2	47	5.790
\vdots	\vdots	\vdots	\vdots
7.06	172.0	847	0.591
7.22	174.1	923	0.558
7.70	179.2	1158	0.459
7.86	181.5	1266	0.435
8.00	183.6	1386	0.413

TABLE III: Sample data from the experiment. At each voltage setting, the current through LED is measured in mA and the LDR’s resistance is measured in k Ω . The experiment is repeated with LDR replaced by a flux meter to measure power.

The model obtained from data (Fig. 14a) suggests potential V as the cause for both power P and current I , and finds no direct causal relation between power P and the LDR resistance R . The model as expected provide only the most significant cause-effect relations (Table IV). We know, as depicted in the domain knowledge model (Fig. 14b), that current I acts as a mediator for V ’s effect on P . This becomes clear when we compare refutations of models with and without $I \rightarrow P$ arm. Refutations suggest that we put more faith in the model with $I \rightarrow P$ arm (p-value 0.912) than the ones without this arm (p-value 0.882) (Table V). The analysis also suggest that we put more faith in the model which includes the $P \rightarrow R$ arm over the one that does not contain this arm.

D. Measurement correlation and quantum entanglement

The last example we choose is from the domain of quantum mechanics. Quantum states of composite

Model	Estimates (ATE)		
	$V \rightarrow P$	$V \rightarrow I$	$P \rightarrow R$
Data	251.533	15.42	-
Domain Knowledge	251.533	15.41	-0.008

TABLE IV: Causal estimates of three causal relations for data and the domain knowledge models in the LDR experiment

	$P \rightarrow R$ present	$P \rightarrow R$ absent
$I \rightarrow P$ present	0.928	0.896
$I \rightarrow P$ absent	0.897	0.867

TABLE V: Confidence levels of $V \rightarrow P$ causal estimate for different causal models in the LDR experiment

systems can show peculiar kinds of correlations. We analyze these correlations from the point of view of constructing a causal model.

A quantum spin half particle is a two level quantum system with its state space consisting of normalized densities over a two dimensional complex linear vector space. [48] The measurables for each particle are spin components in any direction and the spin component takes two values ‘up’(1) or ‘down’(0) when measured and are the eigen values of the corresponding Hermitian operator. For example if we are measuring the z component of spin the corresponding observable is the Pauli matrix σ_z . The scenario that we consider consists of two spin half particles which are in a joint quantum state ρ . Alice and Bob are two observers with the capability of measuring spin components and the first particle is accessible to Alice while the second is accessible to Bob. The scenario is schematically depicted in Fig. 15.

Consider the case where both Alice and Bob measure the spin of their respective particle along the z -axis which corresponds to measuring the operator σ_z in the appropriate state space. For each the possible outcomes thus are 0 or 1. Therefore, the joint measurement outcome for the composite system will be in the set $\{00,01,10,11\}$. One can compare this situation to the one of tossing two coins in the classical domain where the outcome set is the same and if the coins are unbiased, the probability of each outcome will be equal.

Quantum states have a property called quantum entanglement [49] which is considered to be responsible for unusual correlation properties of composite quantum systems. The entanglement can be mathematically computed from the given density operator and can be quantified via a measure called log-

negativity [50]. For certain maximally entangled states the outcomes can be such that they always either fall in the set $\{01,10\}$ or the set $\{00,11\}$, *i.e.* the outcomes are always (anti)correlated. This scenario is schematically described in Fig. 15. The data set

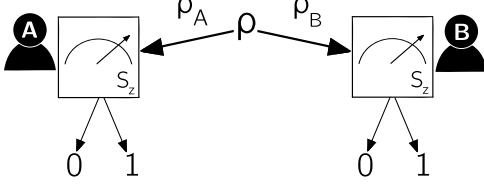


FIG. 15: Alice and Bob with a shared quantum state ρ of two spin half particles. Each measures the spin of their particle along the z -axis and gets one of two possible outcomes (0 or 1).

the we analyze is generated by simulating the measurement setup between Alice and Bob. A state of the composite quantum system ρ is generated randomly. On this randomly generated state, both Alice and Bob, perform a σ_z measurement. They repeat these measurements on the state 100 times and these 100 measured values are used to compute the correlation. The entanglement is computed from the state density matrix mathematically by computing the log-negativity. This process is repeated for another randomly generated composite state of the two spins. Twenty such random states are chosen and thus a data-set with 2000 rows is generated with 100 rows corresponding to a given random state ρ . The data set is schematically described in Table VI. As can be seen for each ρ we have 100 rows which are used to calculate the correlations and have mathematically computed log-negativities as documented in the second column.

Where is the cause of the correlation between the measured values of Alice and Bob? The initial causal discovery attempts failed to reveal any relations between the variables. Upon further investigation into the data, we find that the present scenario is a special case where the variables of interest, though causally linked (as we know from Domain knowledge), have zero correlation between them. Entanglement ranging from 0 to 1, while Correlation ranging from -1 to +1 creates a case where the average correlation between these two variables is (very close to) zero.

Tackling such cases involves looking at the causal relation among functions of the involved variables. We take the absolute value of correlation as the second variable of interest and continue with the analysis. Similar to the tide-height example, the predicted causal diagram only shows the most significant cause-effect relation. With M_A as the treat-

State	Entanglement	M_A	M_B	Correlation	
ρ_1	E_1	+1	-1	C_1	instance 1 (100 rows)
..	
ρ_1	E_1	-1	-1	C_1	
ρ_2	E_2	+1	+1	C_2	instance 2 (100 rows)
..	
ρ_2	E_2	-1	+1	C_2	
..	
..	
ρ_n	E_n	-1	+1	C_n	instance n (100 rows)
..	
ρ_n	E_n	+1	+1	C_n	

TABLE VI: Structural setup of the data generated in the simulation of Alice and Bob's σ_z measurements on two entangled spin half particles. A single instance is 100 samples of measurements performed by Alice (M_A) and Bob (M_B) on the shared state ρ . The correlation value C is evaluated from these 100 samples.

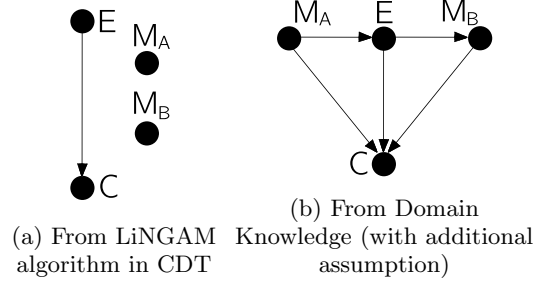


FIG. 16: Causal diagram for correlation between Alice and Bob's measurement outcomes (M_A and M_B respectively).

ment and correlation (C) as the outcome (while accounting for entanglement(E) as a common cause), we get a causal estimate of -0.0002 ATE. Similarly, we get -0.0024 ATE for M_B (Table VII).

The estimate for entanglement E as the treatment is 0.3733 ATE. This shows that the machine puts more faith in the model that has Entanglement (E), as the underlying variable as the cause of the correlation (C) between M_A and M_B over the model that assumes either M_A or M_B as the cause for C . Therefore, the ML analysis confirms this fact that we know from the domain knowledge.

This statement is further strengthened by the results of refuting the causal model in both the above scenarios. For example, the placebo treatment refutation gives a confidence of 94% (p-value: 0.94) in

Causal Relation	Estimate (ATE)	Confidence (p-value)
$M_A \rightarrow C$	-0.0002	0.82
$M_B \rightarrow C$	-0.0024	0.72
$E \rightarrow C$	0.3733	0.94

TABLE VII: Causal estimates for measurement correlation and entanglement. The p-values are averaged over three different refutation methods.

the former model and a p-value of ~ 0.8 for the latter.

IV. DISCUSSION AND FUTURE WORK

While standard AI and ML based techniques have an outstanding performance in association level tasks, they are unable provide answers to basic queries of cause and effect. One requires the use of causal diagrams and causal inference to equip the machine with said capability. Association level inference is possible even for a machine that understands cause-and-effect relation. Section III A shows that using causal analysis framework one can infer that while both Sun and Moon’s gravitational pull affects the tides on Earth, the Earth-Moon distance is the major cause for the height of tides. The advantage of causal models over simple associative models is seen in Section III B. Not only does the machine estimates potential to be the primary cause for current, it refutes the incorrect assumption of temperature *directly* affecting the current. The LDR experiment

analysis shows that, while the conclusions are not 100% accurate, using causal discovery to infer causal relations from experimental data can hint at where the focus in the experiment should be. In the problem related to cause of correlations between quantum measurements, we observe that the machine is able to figure out the underlying cause of the correlation between the measurement outcomes of Alice and Bob being the quantum entanglement.

Causal Theory is still in its initial stages of development and therefore is in no way foolproof. There exist quite a few different algorithms for causal discovery and there is no guarantee of the outcomes of one agreeing with the outcomes of the other. The approach is data-centric and does not always yield relations that make sense. Nonetheless, having an initial estimate of a causal model helps speed up the process. One can always fine-tuned the estimates and relations using domain knowledge. Adding the layer of causal analysis can deepen the understanding of the phenomena and processes involved. The authors in [51] present a physics-inspired symbolic regression ML algorithm for discovering expressions/equations from data alone. One can explore the advantage of incorporating causal inference to such ML applications.

ACKNOWLEDGMENTS

J.S. would like to thank Amitoj Kaur Chandi (@nick.naysayer) for Fig. 1 and Dr. Paramdeep Singh for help with the experimental setup for Section III C. J.S. acknowledges IISER Mohali for financial support.

-
- [1] Konstantinos Liakos, Patrizia Busato, Dimitrios Moshou, Simon Pearson, and Dionysis Bochtis, “Machine learning in agriculture: A review,” *Sensors* **18**, 2674 (2018).
- [2] Sheena Angra and Sachin Ahuja, “Machine learning and its applications: A review,” in *2017 International Conference on Big Data Analytics and Computational Intelligence (ICBI-IC)* (2017) pp. 57–60.
- [3] Derrick Mwiti, “10 real-life applications of reinforcement learning,” (2023).
- [4] Giuseppe Carleo and Matthias Troyer, “Solving the quantum many-body problem with artificial neural networks,” *Science* **355**, 602–606 (2017).
- [5] Naeimeh Mohseni, Thomas Fösel, Lingzhen Guo, Carlos Navarrete-Benlloch, and Florian Marquardt, “Deep Learning of Quantum Many-Body Dynamics via Random Driving,” *Quantum* **6**, 714 (2022).
- [6] S. S. Schoenholz, E. D. Cubuk, D. M. Sussman, E. Kaxiras, and A. J. Liu, “A structural approach to relaxation in glassy liquids,” *Nature Physics* **12**, 469–471 (2016).
- [7] Juan Carrasquilla and Roger G. Melko, “Machine learning phases of matter,” *Nature Physics* **13**, 431–434 (2017).
- [8] Kelvin Ch’ng, Juan Carrasquilla, Roger G. Melko, and Elham Khatami, “Machine learning phases of strongly correlated fermions,” *Phys. Rev. X* **7**, 031038 (2017).
- [9] Simone Tibaldi, Giuseppe Magnifico, Davide Vodola, and Elisa Ercolessi, “Unsupervised and supervised learning of interacting topological phases from single-particle correlation functions,” *SciPost Phys.* **14**, 005 (2023).
- [10] Mario Krenn, Mehul Malik, Robert Fickler, Radek Lapkiewicz, and Anton Zeilinger, “Automated search for new quantum experiments,” *Phys. Rev. Lett.* **116**, 090405 (2016).
- [11] Xiaoqin Gao, Manuel Erhard, Anton Zeilinger, and

- Mario Krenn, “Computer-inspired concept for high-dimensional multipartite quantum gates,” *Phys. Rev. Lett.* **125**, 050501 (2020).
- [12] Amin Babazadeh, Manuel Erhard, Feiran Wang, Mehul Malik, Rahman Nouroozi, Mario Krenn, and Anton Zeilinger, “High-dimensional single-photon quantum gates: Concepts and experiments,” *Phys. Rev. Lett.* **119**, 180510 (2017).
- [13] Manuel Erhard, Mehul Malik, Mario Krenn, and Anton Zeilinger, “Experimental greenberger–horne–zeilinger entanglement beyond qubits,” *Nature Photonics* **12**, 759–764 (2018).
- [14] Pascal Friederich, Mario Krenn, Isaac Tamblin, and Alán Aspuru-Guzik, “Scientific intuition inspired by machine learning-generated hypotheses,” *Machine Learning: Science and Technology* **2**, 025027 (2021).
- [15] Daniel Flam-Shepherd, Tony C. Wu, Xuemei Gu, Alba Cervera-Lierta, Mario Krenn, and Alán Aspuru-Guzik, “Learning interpretable representations of entanglement in quantum optics experiments using deep generative models,” *Nature Machine Intelligence* **4**, 544–554 (2022).
- [16] Kishor Bharti, Tobias Haug, Vlatko Vedral, and Leong-Chuan Kwek, “How to teach ai to play bell non-local games: Reinforcement learning,” (2019), arXiv:1912.10783 [quant-ph].
- [17] Giacomo Torlai, Guglielmo Mazzola, Juan Carrasquilla, Matthias Troyer, Roger Melko, and Giuseppe Carleo, “Neural-network quantum state tomography,” *Nature Physics* **14**, 447–450 (2018).
- [18] Matthew J. S. Beach, Isaac De Vlught, Anna Golubeva, Patrick Huembeli, Bohdan Kulchytskyy, Xiuzhe Luo, Roger G. Melko, Ejaaz Merali, and Giacomo Torlai, “QuCumber: wavefunction reconstruction with neural networks,” *SciPost Phys.* **7**, 009 (2019).
- [19] Lei Wang, “Discovering phase transitions with unsupervised learning,” *Phys. Rev. B* **94**, 195105 (2016).
- [20] Wenjian Hu, Rajiv R. P. Singh, and Richard T. Scalettar, “Discovering phases, phase transitions, and crossovers through unsupervised machine learning: A critical examination,” *Phys. Rev. E* **95**, 062122 (2017).
- [21] Juan Carrasquilla, “Machine learning for quantum matter,” *Advances in Physics: X* **5**, 1797528 (2020).
- [22] Li Huang and Lei Wang, “Accelerated monte carlo simulations with restricted boltzmann machines,” *Phys. Rev. B* **95**, 035105 (2017).
- [23] Qianshi Wei, Roger G. Melko, and Jeff Z. Y. Chen, “Identifying polymer states by machine learning,” *Phys. Rev. E* **95**, 032504 (2017).
- [24] Giacomo Torlai and Roger G. Melko, “Neural decoder for topological codes,” *Phys. Rev. Lett.* **119**, 030501 (2017).
- [25] B. P. Abbott, R. Abbott, et al. (LIGO Scientific Collaboration and Virgo Collaboration), “Observation of gravitational waves from a binary black hole merger,” *Phys. Rev. Lett.* **116**, 061102 (2016).
- [26] Thomas Fösel, Murphy Yuezheng Niu, Florian Marquardt, and Li Li, “Quantum circuit optimization with deep reinforcement learning,” (2021), arXiv:2103.07585 [quant-ph].
- [27] Thomas Fösel, Petru Tighineanu, Talitha Weiss, and Florian Marquardt, “Reinforcement learning with neural networks for quantum feedback,” *Phys. Rev. X* **8**, 031084 (2018).
- [28] Koji Hashimoto, Sotaro Sugishita, Akinori Tanaka, and Akio Tomiya, “Deep learning and the ads-cft correspondence,” *Phys. Rev. D* **98**, 046019 (2018).
- [29] Marin Bukov, “Reinforcement learning for autonomous preparation of floquet-engineered states: Inverting the quantum kapitza oscillator,” *Phys. Rev. B* **98**, 224305 (2018).
- [30] Marin Bukov, Alexandre G. R. Day, Dries Sels, Phillip Weinberg, Anatoli Polkovnikov, and Pankaj Mehta, “Reinforcement learning in different phases of quantum control,” *Phys. Rev. X* **8**, 031086 (2018).
- [31] Giacomo Torlai and Roger G. Melko, “Learning thermodynamics with boltzmann machines,” *Phys. Rev. B* **94**, 165134 (2016).
- [32] Yashar D. Hezaveh, Laurence Perreault Levasseur, and Philip J. Marshall, “Fast automated analysis of strong gravitational lenses with convolutional neural networks,” *Nature* **548**, 555–557 (2017).
- [33] Jonathan Carifio, James Halverson, Dmitri Krioukov, and Brent D. Nelson, “Machine learning in the string landscape,” *Journal of High Energy Physics* **2017** (2017), 10.1007/jhep09(2017)157.
- [34] Rahul Biswas, Lindy Blackburn, Junwei Cao, Reed Essick, Kari Alison Hodge, Erotokritos Katsavounidis, Kyungmin Kim, Young-Min Kim, Eric-Olivier Le Bigot, Chang-Hwan Lee, John J. Oh, Sang Hoon Oh, Edwin J. Son, Ye Tao, Ruslan Vaulin, and Xiaoge Wang, “Application of machine learning algorithms to the study of noise artifacts in gravitational-wave data,” *Phys. Rev. D* **88**, 062003 (2013).
- [35] Raban Iten, Tony Metger, Henrik Wilming, Lídia del Rio, and Renato Renner, “Discovering physical concepts with neural networks,” *Phys. Rev. Lett.* **124**, 010508 (2020).
- [36] Judea Pearl and Dana Mackenzie, *The book of why: The new science of cause and effect* (Basic Books, 2020).
- [37] Clark Glymour, Kun Zhang, and Peter Spirtes, “Review of causal discovery methods based on graphical models,” *Frontiers in Genetics* **10** (2019), 10.3389/fgene.2019.00524.
- [38] Markus Kalisch, Martin Mächler, Diego Colombo, Marloes H. Maathuis, and Peter Bühlmann, “Causal inference using graphical models with the r package pcalg,” *Journal of Statistical Software* **47**, 1–26 (2012).
- [39] David Maxwell Chickering, “Optimal structure identification with greedy search,” *J. Mach. Learn. Res.* **3**, 507–554 (2003).
- [40] Shohei Shimizu, Patrik O. Hoyer, Aapo Hyvärinen, and Antti Kerminen, “A linear non-gaussian acyclic model for causal discovery,” *J. Mach. Learn. Res.* **7**, 2003–2030 (2006).
- [41] Emre Kiciman Amit Sharma, “Methods for causal

- inference,” (2018).
- [42] Diviyani Kalainathan, Olivier Goudet, and Ritik Dutta, “Causal discovery toolbox: Uncovering causal relationships in python,” *J. Mach. Learn. Res.* **21** (2020).
- [43] Amit Sharma and Emre Kiciman, “Dowhy: An end-to-end library for causal inference,” *arXiv preprint arXiv:2011.04216* (2020), causal Data Science Meeting (<https://causalscience.org/>).
- [44] Emden Gansner, Eleftherios Koutsofios, Stephen North, *Drawing graphs with dot*, Tech. Rep. (AT & T Research, 2006).
- [45] Paul R. Rosenbaum and Donald B. Rubin, “The central role of the propensity score in observational studies for causal effects,” *Biometrika* **70**, 41–55 (1983).
- [46] Abraham Wald, “Tests of statistical hypotheses concerning several parameters when the number of observations is large,” *Transactions of the American Mathematical Society* **54**, 426–482 (1943).
- [47] Donald L. Thistlethwaite and Donald T. Campbell, “Regression-discontinuity analysis: An alternative to the ex post facto experiment.” *Journal of Educational Psychology* **51**, 309–317 (1960).
- [48] Shinil Cho, “Two-level quantum systems,” in *Quantum Computation and Quantum Information Simulation using Python*, 2053-2563 (IOP Publishing, 2022) pp. 1–1 to 1–14.
- [49] Ryszard Horodecki, Paweł Horodecki, Michał Horodecki, and Karol Horodecki, “Quantum entanglement,” *Rev. Mod. Phys.* **81**, 865–942 (2009).
- [50] Martin B. Plenio and Shashank Virmani, “An introduction to entanglement measures,” *Quantum Info. Comput.* **7**, 1–51 (2007).
- [51] Silviu-Marian Udrescu and Max Tegmark, “Ai feynman: A physics-inspired method for symbolic regression,” *Science Advances* **6**, eaay2631 (2020).

Appendix A: Causal Analysis - DoWhy

DoWhy is “An end-to-end library for causal inference” developed by Microsoft. It abstracts the entire process of causal analysis into a 4 step process: model, identify, estimate, and refute.

Where the general trend of causal inference is estimation of a model parameter like the coefficient of linear regression, DoWhy provides a do-sampler that estimates the distribution of $P(Y|do(X = x))$. This enables us to compute statistics other than test and control difference in average outcomes.

Considering the example of tide heights:

1. Model

One can provide a model as a digraph from the knowledge related to the subject:

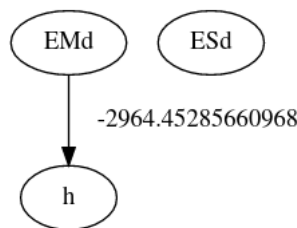
```
causal_graph = '''digraph {
EMd[label='Earth-Moon distance'];
ESd[label='Earth-Sun distance'];
h[label='height of the tide']
ESd->EMd->h;
ESd->h;
}'''
model= dowhy.CausalModel(data = dataset_halifax ,
                           graph=causal_graph.replace('\n', ' '),
                           treatment='EMd',
                           outcome='h',
                           common_causes='ESd')

model.view_model()
display(Image(filename='causal_model.png'))
```

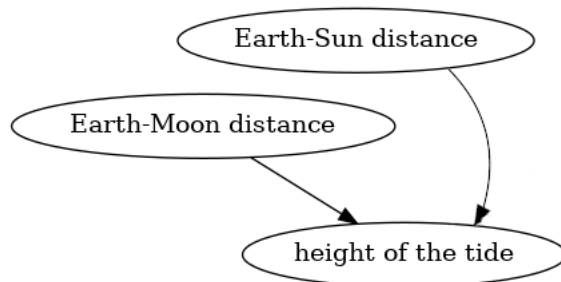
Or one can obtain the model from the data itself using causal discovery algorithms (CDT package):

```
from cdt.causality.graph import LiNGAM
labels = list(dataset_halifax.columns)
predicted_graph = LiNGAM().predict(dataset_halifax)
adj_matrix = np.asarray(nx.to_numpy_matrix(predicted_graph))
idx = np.abs(adj_matrix) > 0.01
dirs = np.where(idx)
graph = graphviz.Digraph(engine='dot')
for name in labels:
    graph.node(name)
for edge_to, edge_from, value in zip(dirs[0], dirs[1], adj_matrix[idx]):
    graph.edge(labels[edge_from], labels[edge_to], label=str(value))
display(graph)
```

Result:



(a) From LiNGAM algorithm in CDT



(b) From Domain Knowledge

2. Identify

```
import statsmodels
identified_estimand = model.identify_effect(
    proceed_when_unidentifiable=True)
print(identified_estimand)
```

Result:

Estimand type: nonparametric-ate

```
### Estimand : 1
Estimand name: backdoor
Estimand expression:
d
-----
(EExpectation(h))
d[ESd]
Estimand assumption 1, Unconfoundedness: If  $U \perp \{ESd\}$  and  $U \perp h$ 
then  $P(h|ESd, U) = P(h|ESd)$ 
```

```
### Estimand : 2
Estimand name: iv
No such variable found!
```

```
### Estimand : 3
Estimand name: frontdoor
No such variable found!
```

3. Estimate

```
estimate = model.estimate_effect(identified_estimand,
    method_name='backdoor.linear_regression',
    control_value=0,
    treatment_value=1,
    confidence_intervals=True,
    test_significance=True)
print('Estimate:', estimate.value)
```

Result:

Estimate: -2913.157882942987

4. Refute

```
# Placebo Treatment Refuter:— Randomly assigns any covariate as
# a treatment and re-runs the analysis. If our assumptions were
# correct then this newly found out estimate should go to 0.
refute = model.refute_estimate(identified_estimand, estimate,
    method_name='placebo_treatment_refuter')
print(refute)
```

Result:

Refute: Use a Placebo Treatment
 Estimated effect: -2913.157882942987
 New effect: 0.0
 p value: 1.0